

Iron Catalyst Chemistry in Modeling a High-Pressure Carbon Monoxide Nanotube Reactor

Carl D. Scott,^{a,*} Alexander Povitsky,^b Christopher Dateo,^c Tahir Gökçen,^c
Peter A. Willis,^d and Richard E. Smalley^d

^aNASA Johnson Space Center, Houston, Texas, USA

^bICASE, NASA Langley Research Center, Hampton, Virginia, USA

^cEloret Corporation, NASA Ames Research Center, Moffatt Field, California, USA

^dCenter for Nanoscale Science and Technology, Rice University, Houston, Texas, USA

The high-pressure carbon monoxide (HiPco) technique for producing single-wall carbon nanotubes (SWNTs) is analyzed with the use of a chemical reaction model coupled with flow properties calculated along streamlines, calculated by the FLUENT code for pure carbon monoxide. Cold iron pentacarbonyl, diluted in CO at about 30 atmospheres, is injected into a conical mixing zone, where hot CO is also introduced via three jets at 30° with respect to the axis. Hot CO decomposes the Fe(CO)₅ to release atomic Fe. Then iron nucleates and forms clusters that catalyze the formation of SWNTs by a disproportionation reaction (Boudouard) of CO on Fe-containing clusters. Alternative nucleation rates are estimated from the theory of hard sphere collision dynamics with an activation energy barrier. The rate coefficient for carbon nanotube growth is estimated from activation energies in the literature. The calculated growth was found to be about an order of magnitude greater than measured, regardless of the nucleation rate. A study of cluster formation in an incubation zone prior to injection into the reactor shows that direct dimer formation from Fe atoms is not as important as formation via an exchange reaction of Fe with CO in FeCO.

Keywords: Single-Wall Carbon Nanotubes, HiPco, Nanotube Reactor, Iron Catalyst.

1. INTRODUCTION

The high-pressure process for the production of single-wall carbon nanotubes (SWNTs) was developed by Nikolaev et al.¹ at Rice University and was studied parametrically.² The process converts carbon monoxide into SWNTs and CO₂ at about 30 bar (3 MPa) and about 1000 °C from the so-called Boudouard reaction on iron catalyst particles. The process has been given the name HiPco. Iron particles are liberated from iron pentacarbonyl (Fe(CO)₅) when it decomposes above about 250 °C. The free iron then forms clusters that catalyze the Boudouard reaction. It is presumed that the rate of formation and the size and number of iron clusters have a significant effect on the amount and purity of the product SWNTs. Iron pentacarbonyl, diluted in room-temperature CO, is injected into a conical mixing region in which hot (1150 °C) CO is injected. This zone of the reactor is called the "shower head." Figure 1 shows the general arrangement of the shower head and some of the upstream and downstream portions of the reactor. It is the purpose of this paper to understand what factors influence the growth and purity of the product SWNTs and to investigate ways of improving the process.

The paper includes (1) a description of the geometry and operation of the process; (2) a brief description of the fluid dynamics simulation; (3) the chemical reaction models used to compute iron cluster formation and growth, and nanotube formation and growth; (4) a comparison of nucleation models, a comparison of cluster growth models and coupling of these chemical rate models with the flow field results; (5) a comparison of SWNT and CO₂ formation with measurements; and (6) an investigation of an incubation zone in which cold dilute Fe(CO)₅ is initially dissociated (as by a laser).

2. EXPERIMENTAL DETAILS

2.1. Apparatus Description

Inside a thick-walled cylindrical aluminum chamber the flow reactor consists of a silica or alumina tube surrounded by heating elements. Iron pentacarbonyl vapor carried by near-room-temperature carbon monoxide is injected into the apex of the conical inlet of the reactor through a water-cooled copper injector with an inner diameter of 1 mm. (see Fig. 1). Carbon monoxide, heated by electric heating elements, is injected through three 1-mm-diameter orifices in the sidewall of a graphite cone.

* Author to whom correspondence should be addressed.

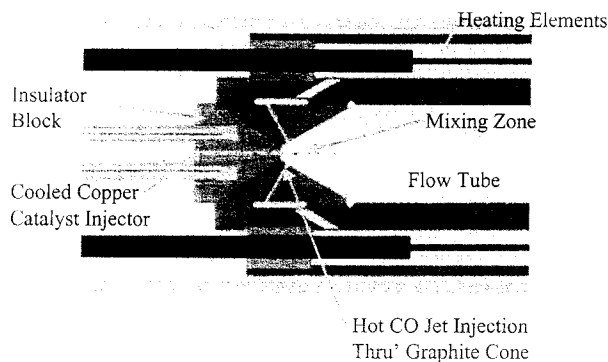


Fig. 1. Schematic of HiPco reactor injection and mixing zones.

The cold and hot gases mix quickly in the conical and downstream cylindrical zones, and the cold $\text{Fe}(\text{CO})_5$ is heated and diluted and decomposes. In the analysis of this paper, we have considered only a three-port injector. It was determined from early computational fluid dynamics simulations that three ports did a better job of mixing than two or six ports. The inner diameter of the cylindrical reactor tube is 2.5 cm. Although its actual heated length is about 61 cm, it was assumed to be only 20 cm in the present calculations; beyond that the tube is assumed to be cooled to room temperature. The heated length did not appear to have a significant effect on the calculated product. The ratio of catalyst flow to hot CO flow is assumed to be 1:3 in the calculations. The mole fraction of $\text{Fe}(\text{CO})_5$ in the cold inlet ranges from 3.2 to 32 ppm, and in some calculations it was assumed to be 17×10^{-6} . The flow rate of the cold gas was 1.4 liters/min or 42 slm.

2.2. Fluid Dynamics Simulation

The flow field in the mixing zone and reactor tube is determined from numerical solutions of the Navier-Stokes equations at points defined by a numerical mesh. Three-fold symmetry was assumed for the three-dimensional calculation with the FLUENT code.^{3,4} The steady Navier-Stokes equations for a nonreacting gas were solved, assuming a $k-\epsilon$ turbulence model. Based on the Reynolds number, the flow would be transitional; but turbulence was expected because of the violent interaction of the jets. Because of the very high dilution of iron, the flow chemistry could be considered fully decoupled from the fluid dynamics. That is, chemical reactions should have a negligible effect on the flow. From the solution, streamlines were determined in the flow; and the temperature history along the streamlines was determined for use in solving the chemical rate equations in a separate calculation. Since the turbulence model used in the flow field solution yields only average values and does not include local fluctuations, the temperature is essentially averaged over the turbulent fluctuations. Because the chemical rates

are sensitive to temperature, some effects of turbulence may not be represented by these solutions.

The chemical rate equations

$$\frac{dn_i}{dt} = \sum_r \left[k_{fr} \prod_k n_k^{\nu'_{kr}} - k_{br} \prod_k n_k^{\nu''_{kr}} \right] (\nu'_{ir} - \nu''_{ir}) \quad (1)$$

were solved for the density n_i (or concentration) of species i , where k_{fr} and k_{br} are the forward and reverse reaction rate coefficients for reaction r , and ν'_{kr} and ν''_{kr} are, respectively, the reactant and product stoichiometric coefficients of species k and reaction r . These equations were solved simultaneously with the program SENKIN (Ref. 5) of the CHEMKIN 3.6 package.

2.3. Chemical Kinetics Models

Several variations of the chemical kinetics model are examined in terms of the size of clusters considered, cluster growth rates, and the rate of nucleation of Fe to form Fe_2 .

2.3.1. Cluster Options. The first model was developed at NASA Ames Research Center with inputs from Daniel Colbert of Rice University. It contains 971 species and 2150 reactions. This paper calls this model the "Ames Preliminary Model." (NASA Ames Research Center has developed a more recent model for nanotube growth, published in Ref. 6. This model was not available for the present calculations; therefore, their preliminary model is used.) It contains decomposition reactions for the family of iron carbonyls that are the same for all models considered. It considers an assumed Fe nucleation rate, the growth of Fe_n and Fe_nCO clusters, and conversion of Fe_nCO clusters to SWNTs (each assumed to have an average number of 999 carbon atoms in the present calculations), and Fe clusters and SWNTs that have ceased to grow because of some poisoning mechanism (dead clusters) are denoted DCNT_n and DFe_n , respectively. Table Ia gives the reaction model in shortened form. The notation CNT_n denotes a carbon nanotube attached to an iron cluster. The subscript n denotes the number of iron atoms in the cluster. Agglomeration is limited to the addition of Fe, Fe_2 , Fe_3 , and Fe_4 .

The second and third models are based on the iron pentacarbonyl and nanotube growth reactions of the Ames preliminary model and on the Girshick model for cluster growth and evaporation. Unlike the Ames preliminary model, these models allow for coagulation of clusters with $n > 4$. The second model is truncated at $n = 40$. Table Ib gives the reactions and rate coefficients for this scheme. To reduce the total number of species, a third model considered (shown in Table Ic) contains clusters up to $n = 2048$ atoms. There are clusters for $n = 2, 3, \dots, 7, 8, 16, 32, 64, 128, 256, 512, 1024$, and 2048. Cluster formation rates of Rao et al.⁷ (referred to as Girshick rates) in the latter two models are estimated from

Table I. Nanotube Model Reaction Schemes.

a) Ames Model up to 200-Atom Clusters				b) Girshick Based Model up to 40-Atom Clusters				c) Girshick Based Nanotube Cluster Model up to 2048-Atom Clusters			
Reaction	A	η	Ea	Reaction	A	η	Ea	Reaction	A	η	Ea
1. Iron Carbonyl Reactions (Ames)											
$\text{Fe}(\text{CO})_5 \Rightarrow \text{Fe}(\text{CO})_4 + \text{CO}$	4.62E+20	-1.96	21028.3	$\text{Fe}(\text{CO})_5 \Rightarrow \text{Fe}(\text{CO})_4 + \text{CO}$	4.62E+20	-1.96	21028.3	$\text{Fe}(\text{CO})_5 \Rightarrow \text{Fe}(\text{CO})_4 + \text{CO}$	4.62E+20	-1.96	21028.3
$\text{Fe}(\text{CO})_4 + \text{CO} \Rightarrow \text{Fe}(\text{CO})_5$	3.50E+10	0	0	$\text{Fe}(\text{CO})_4 + \text{CO} \Rightarrow \text{Fe}(\text{CO})_5$	3.50E+10	0	0	$\text{Fe}(\text{CO})_4 + \text{CO} \Rightarrow \text{Fe}(\text{CO})_5$	3.50E+10	0	0
$\text{Fe}(\text{CO})_3 + \text{CO} \Rightarrow \text{Fe}(\text{CO})_4$	6.96E+22	-2.14	14346.3	$\text{Fe}(\text{CO})_3 + \text{CO} \Rightarrow \text{Fe}(\text{CO})_4$	6.96E+22	-2.14	14346.3	$\text{Fe}(\text{CO})_3 + \text{CO} \Rightarrow \text{Fe}(\text{CO})_4$	6.96E+22	-2.14	14346.3
$\text{Fe}(\text{CO})_2 + \text{CO} \Rightarrow \text{Fe}(\text{CO})_3$	1.30E+13	0	0	$\text{Fe}(\text{CO})_2 + \text{CO} \Rightarrow \text{Fe}(\text{CO})_3$	1.30E+13	0	0	$\text{Fe}(\text{CO})_2 + \text{CO} \Rightarrow \text{Fe}(\text{CO})_3$	1.30E+13	0	0
$\text{Fe}(\text{CO})_5 \Rightarrow \text{Fe}(\text{CO})_2 + \text{CO}$	8.70E+19	-1.58	14679.8	$\text{Fe}(\text{CO})_5 \Rightarrow \text{Fe}(\text{CO})_2 + \text{CO}$	8.70E+19	-1.58	14679.8	$\text{Fe}(\text{CO})_5 \Rightarrow \text{Fe}(\text{CO})_2 + \text{CO}$	8.70E+19	-1.58	14679.8
$\text{Fe}(\text{CO})_4 \Rightarrow \text{Fe}(\text{CO})_2 + \text{CO}$	1.80E+13	0	0	$\text{Fe}(\text{CO})_4 \Rightarrow \text{Fe}(\text{CO})_2 + \text{CO}$	1.80E+13	0	0	$\text{Fe}(\text{CO})_4 \Rightarrow \text{Fe}(\text{CO})_2 + \text{CO}$	1.80E+13	0	0
$\text{Fe}(\text{CO})_3 \Rightarrow \text{Fe}(\text{CO})_2 + \text{CO}$	3.96E+21	-2.29	18799.4	$\text{Fe}(\text{CO})_3 \Rightarrow \text{Fe}(\text{CO})_2 + \text{CO}$	3.96E+21	-2.29	18799.4	$\text{Fe}(\text{CO})_3 \Rightarrow \text{Fe}(\text{CO})_2 + \text{CO}$	3.96E+21	-2.29	18799.4
$\text{FeCO} + \text{CO} \Rightarrow \text{Fe}(\text{CO})_2$	1.50E+13	0	0	$\text{FeCO} + \text{CO} \Rightarrow \text{Fe}(\text{CO})_2$	1.50E+13	0	0	$\text{FeCO} + \text{CO} \Rightarrow \text{Fe}(\text{CO})_2$	1.50E+13	0	0
$\text{FeCO} + \text{M} \Rightarrow \text{Fe} + \text{CO} + \text{M}$	4.87E+19	-0.9	2874.5	$\text{FeCO} + \text{M} \Rightarrow \text{Fe} + \text{CO} + \text{M}$	4.87E+19	-0.9	2874.5	$\text{FeCO} + \text{M} \Rightarrow \text{Fe} + \text{CO} + \text{M}$	4.87E+19	-0.9	2874.5
$\text{Fe} + \text{CO} + \text{M} \Rightarrow \text{FeCO} + \text{M}$	1.00E+15	0	0	$\text{Fe} + \text{CO} + \text{M} \Rightarrow \text{FeCO} + \text{M}$	1.00E+15	0	0	$\text{Fe} + \text{CO} + \text{M} \Rightarrow \text{FeCO} + \text{M}$	1.00E+15	0	0
$\text{FeCO} + \text{FeCO} \Rightarrow \text{Fe}_2 + \text{CO} + \text{CO}$	6.00E+14	0	1006.43	$\text{FeCO} + \text{FeCO} \Rightarrow \text{Fe}_2 + \text{CO} + \text{CO}$	6.00E+14	0	1006.43	$\text{FeCO} + \text{FeCO} \Rightarrow \text{Fe}_2 + \text{CO} + \text{CO}$	6.00E+14	0	1006.43
2. Fe Nucleation*											
$\text{Fe} + \text{Fe} + \text{M} \Rightarrow \text{Fe}_2 + \text{M}$	1.00E+20	0	0	$\text{Fe} + \text{Fe} \Rightarrow \text{Fe}_2$	4.58E+12	0.5	0	$\text{Fe} + \text{Fe} \Rightarrow \text{Fe}_2$	4.58E+12	0.5	0
$\text{Fe}_2 + \text{Fe} + \text{M} \Rightarrow \text{Fe}_3 + \text{M}$	1.00E+20	0	0	Collision frequency model*				Collision frequency model†			
3. Fe-atom Exchange											
$\text{Fe}_2 + \text{Fe}_2 \Rightarrow \text{Fe}_3 + \text{Fe}$	3.00E+14	0	0	$\text{Fe}_2 + \text{Fe}_2 \Rightarrow \text{Fe}_3 + \text{Fe}$	3.00E+14	0	0	$\text{Fe}_2 + \text{Fe}_2 \Rightarrow \text{Fe}_3 + \text{Fe}$	3.00E+14	0	0
$\text{Fe}_2 + \text{Fe}_3 \Rightarrow \text{Fe}_4 + \text{Fe}$	3.00E+14	0	0	$\text{Fe}_2 + \text{Fe}_3 \Rightarrow \text{Fe}_4 + \text{Fe}$	3.00E+14	0	0	$\text{Fe}_2 + \text{Fe}_3 \Rightarrow \text{Fe}_4 + \text{Fe}$	3.00E+14	0	0
4. Fe-Cluster Growth											
$\text{Fe}_n + \text{Fe}_n \Rightarrow \text{Fe}_{(n+1)}$	k/bn, n+1			$\text{Fe}_n + \text{Fe}_n \Rightarrow \text{Fe}_{(n+1)}$	k/bn, n+1			$\text{Fe}_n + \text{Fe}_n \Rightarrow \text{Fe}_{(n+1)}$	k/bn, n+1		
$\text{Fe}_3 + \text{Fe}_n \Rightarrow \text{Fe}_{(n+3)}$	3.30E+14	0.5	0	$3 \leq n \leq 195$	4.97E+12	0.5	0	$2 \leq n \leq 39$	4.97E+12	0.5	0
$\text{Fe}_2 + \text{Fe}_n \Rightarrow \text{Fe}_{(n+2)}$	3.29E+14	0.5	0	$2 \leq n \leq 198$				$\text{Fe}_n + \text{Fe}_n \Rightarrow \text{Fe}_{(2n)}$			
$\text{Fe}_1 + \text{Fe}_n \Rightarrow \text{Fe}_{(n+1)}$	3.51E+14	0.5	0	$3 \leq n \leq 197$							
$\text{Fe}_4 + \text{Fe}_n \Rightarrow \text{Fe}_{(n+4)}$	3.54E+14	0.5	0	$4 \leq n \leq 196$							
5. Fe-Cluster Evaporation											
$\text{Fe}_2 + \text{M} \Rightarrow \text{Fe} + \text{Fe} + \text{M}$	1.00E+16	0	16102.93	$\text{Fe}_2 \Rightarrow \text{Fe} + \text{Fe}$	k/bn, n+1			$\text{Fe}_n + \text{Fe}_n \Rightarrow \text{Fe}_{(n-1)} + \text{Fe}$	k/bn, n+1		
$\text{Fe}_3 + \text{M} \Rightarrow \text{Fe}_2 + \text{Fe} + \text{M}$	1.00E+16	0	22141.54	$\text{Fe}_3 \Rightarrow \text{Fe}_2 + \text{Fe}$	3.36E+17	-0.5	29.537	$\text{Fe}_n + \text{Fe}_n \Rightarrow \text{Fe}_{(n-1)} + \text{Fe}$	3.36E+17	-0.5	29.537
$\text{Fe}_4 \Rightarrow \text{Fe}_3 + \text{Fe}$	1.00E+13	0	27676.92	$\text{Fe}_4 \Rightarrow \text{Fe}_3 + \text{Fe}$	3.71E+17	-0.5	32.411				
$\text{Fe}_5 \Rightarrow \text{Fe}_4 + \text{Fe}$	2.00E+14	0	30696.22								
$\text{Fe}_6 \Rightarrow \text{Fe}_5 + \text{Fe}$	2.00E+15	0	32709.09								
$\text{Fe}_7 \Rightarrow \text{Fe}_6 + \text{Fe}$	5.00E+15	0	33715.52								
$\text{Fe}_8 \Rightarrow \text{Fe}_7 + \text{Fe}$	1.00E+16	0	34218.74								
$\text{Fe}_9 \Rightarrow \text{Fe}_8 + \text{Fe}$	4.30E+16	0	35225.17								
6. Fe_nCO formation											
$\text{Fe}_n + \text{CO} \Rightarrow \text{Fe}_n\text{CO}$	1.00E+16	0	0	$\text{Fe}_n + \text{CO} \Rightarrow \text{Fe}_n\text{CO}$	1.00E+16	0	0	$\text{Fe}_n + \text{CO} \Rightarrow \text{Fe}_n\text{CO}$	1.00E+16	0	0
$\text{Fe}_n + \text{CO} \Rightarrow \text{Fe}_n\text{CO}$	1.00E+16	0	0	$10 \leq n \leq 200$				$\text{Fe}_n + \text{CO} \Rightarrow \text{Fe}_n\text{CO}$	1.00E+16	0	0
7. Fe_nCO evaporation											
$\text{Fe}_n\text{CO} \Rightarrow \text{Fe}_n + \text{CO}$	1.00E+16	0	16,000	$\text{Fe}_n\text{CO} \Rightarrow \text{Fe}_n + \text{CO}$	1.00E+16	0	16,000	$\text{Fe}_n\text{CO} \Rightarrow \text{Fe}_n + \text{CO}$	1.00E+16	0	16,000
$\text{Fe}_n\text{CO} \Rightarrow \text{Fe}_n + \text{CO}$	1.00E+16	0	16,000	$10 \leq n \leq 200$				$\text{Fe}_n\text{CO} \Rightarrow \text{Fe}_n + \text{CO}$	1.00E+16	0	16,000
8. Fe-CO Exchange											
$\text{Fe} + \text{FeCO} \Rightarrow \text{Fe}_2 + \text{CO}$	6.00E+14	0	0	$\text{Fe} + \text{FeCO} \Rightarrow \text{Fe}_2 + \text{CO}$	6.00E+14	0	0	$\text{Fe}_n + \text{FeCO} \Rightarrow \text{Fe}_{(n+1)} + \text{CO}$	6.00E+14	0	0
$\text{Fe}_2 + \text{FeCO} \Rightarrow \text{Fe}_3 + \text{CO}$	6.00E+14	0	0	$\text{Fe}_2 + \text{FeCO} \Rightarrow \text{Fe}_3 + \text{CO}$	6.00E+14	0	0	$\text{Fe}_n + \text{FeCO} \Rightarrow \text{Fe}_{(n+1)} + \text{CO}$	6.00E+14	0	0
$\text{Fe}_3 + \text{FeCO} \Rightarrow \text{Fe}_4 + \text{CO}$	6.00E+14	0	0	$\text{Fe}_3 + \text{FeCO} \Rightarrow \text{Fe}_4 + \text{CO}$	6.00E+14	0	0	$\text{Fe}_n + \text{FeCO} \Rightarrow \text{Fe}_{(n+1)} + \text{CO}$	6.00E+14	0	0
$\text{Fe}_4 + \text{FeCO} \Rightarrow \text{Fe}_5 + \text{CO}$	6.00E+14	0	0	$\text{Fe}_4 + \text{FeCO} \Rightarrow \text{Fe}_5 + \text{CO}$	6.00E+14	0	0	$\text{Fe}_n + \text{FeCO} \Rightarrow \text{Fe}_{(n+1)} + \text{CO}$	6.00E+14	0	0
$\text{Fe}_n + \text{FeCO} \Rightarrow \text{Fe}_{(n+1)} + \text{CO}$	2.30E+13	0	0	$5 \leq n \leq 200$				$\text{Fe}_n + \text{FeCO} \Rightarrow \text{Fe}_{(n+1)} + \text{CO}$	2.30E+13	0	0

continued

RESEARCH ARTICLE

Table I. Continued

a) Ames Model up to 200-Atom Clusters		b) Girshick Based Model up to 40-Atom Clusters		c) Girshick Based Lumped Cluster Model up to 2048-Atom Clusters	
9. Carbon Nanotube Formation $Fe_nCO + CO \rightarrow (1 - \beta)Fe_nCO + (1 + \beta)/2CO_2 + \beta Fe_nCNT$ $\beta = 1/(2N - 1)$ $N = \text{No. of Carbon atoms in Mean Nanotube}$ $N = 3000$	1.00E+16	0	12,500	1.00E+16	0
10. Poisoning of Fe $Fe_n \Rightarrow DFe_n$	1.00E+03	0	0	$k/bn, n+1$ 6.52E+12	0
13. Poisoning of CNT $CnT \Rightarrow DCnT$	1.00E+00	0	0	$k/bn, n+1$ 7.53E+12	0
9. Carbon Nanotube Formation $Fe_nCO + CO \rightarrow (1 - \beta)Fe_nCO + (1 + \beta)/2CO_2 + \beta Fe_nCNT$ $\beta = 1/(2N - 1)$ $N = \text{No. of Carbon atoms in Mean Nanotube}$ $N = 999$	1.00E+16	0	12,500	1.00E+16	0
10. Fe_n, Fe_m CO Agglomeration $Fe_nCO + Fe_m \Rightarrow Fe_{(n+m)}CO$	$k/bn, n+1$ 6.52E+12	0	0	$k/bn, n+1$ 6.52E+12	0
11a. Fe_n, Fe_m CO-Exchange Cluster Growth $Fe_nCO + Fe_mCO \Rightarrow Fe_{(n+m)}CO + CO$	$k/bn, n+1$ 7.53E+12	0.5	0	$k/bn, n+1$ 7.53E+12	0
11b. Fe_n, Fe_m CO-Exchange Cluster Growth $Fe_nCO + Fe_mCO \Rightarrow Fe_{(n+m)}CO + CO$	$k/bn, n+1$ 7.53E+12	0.5	0	$k/bn, n+1$ 7.53E+12	0
9. Carbon Nanotube Formation $Fe_nCO + CO \rightarrow (1 - \beta)Fe_nCO + (1 + \beta)/2CO_2 + \beta Fe_nCNT$ $\beta = 1/(2N - 1)$ $N = \text{No. of Carbon atoms in Mean Nanotube}$ $N = 999$	1.00E+16	0	12,500	1.00E+16	0
10. Fe_n, Fe_m CO Agglomeration $Fe_nCO + Fe_m \Rightarrow Fe_{(n+m)}CO$	$k/bn, n+1$ 6.52E+12	0	0	$k/bn, n+1$ 6.52E+12	0
11. Fe_n, Fe_m CO-Exchange Cluster Growth $Fe_nCO + Fe_mCO \Rightarrow Fe_{(n+m)}CO + CO$	$k/bn, n+1$ 7.53E+12	0.5	0	$k/bn, n+1$ 7.53E+12	0

*Various nucleation models used.

collision frequencies based on cross sections, assuming spherical symmetry. All models include attachment of CO to iron clusters from $n = 8$. Clusters smaller than $n = 4$ do not have CO attached as indicated by Ref. 8 (at least for the very low pressures of about 1.6 kPa, considered in that paper). A single CO molecule attached is representative, but measurements in Ref. 7 indicate that only one CO is attached to an iron cluster up to at least $n = 14$. More than one CO may be attached to an iron cluster. However, those molecules were not included in the Ames preliminary model, nor were they included here.

Another difference between these models and the Ames preliminary model is the neglect of dead clusters, $DCNT_n$ and DFe_n . In cases where the mole fraction of $Fe_{n_{max}}CO$ becomes larger than that of the smaller clusters, the formation of CNT_n may be overpredicted. However, neglect of these dead species did not seem to have a large influence on CO_2 production.

2.3.2. Summary of Reaction Types. To describe the reaction models in a concise form various categories of reactions are grouped as follows: (1) decomposition and formation of iron carbonyls, (2) nucleation of Fe to form Fe_2 , (3) exchange reactions of Fe and small Fe clusters, (4) attachment of Fe atoms and agglomeration of small Fe molecules to form larger Fe clusters, (5) evaporation of Fe from Fe clusters, (6) attachment of CO to Fe clusters, (7) evaporation (dissociation) of CO from Fe_nCO clusters, (8) Fe-CO exchange, (9) conversion of Fe_nCO clusters to SWNTs (Boudouard reaction), (10) agglomeration of Fe_nCO with Fe_m to form larger clusters, (11) dissociative agglomeration of Fe_nCO to form larger clusters, (12) formation of inert (dead) Fe_n clusters, and (13) formation of inert (dead) SWNTs. Not all categories of reactions were included in all variations of the chemical reaction models. Three variations of the models are given in Table I. These are the original Ames model, the 40-iron-atom cluster model (based on Girshick's cluster rates), and the binary (up to 2048 atoms) cluster model (also based on Girshick's cluster rates). In all three models, iron carbonyl reaction rates and Boudouard reaction rates are taken from the Ames preliminary model. Variations of these models include different assumptions about nucleation rates, discussed in the next section.

2.3.3. Nucleation Options. Four estimates of the nucleation rates were studied. As mentioned, the Ames model assumed a sufficiently high rate to ensure a large rate of formation of nuclei. It is slightly lower than the kinetic collision rate used by Rao et al.⁷ These rates are well above the second one considered, the nucleation rate determined by Krestinin et al.⁹ based on shock tube measurements. It is believed that Fe atoms are difficult to nucleate because of their closed outer electron shell. Therefore, it is necessary to overcome an energy barrier that is sufficient at least to excite an electron to a higher

rate. Hence, the third source of the rate (called “activation barrier nucleation”) is an estimate based on simple hard sphere collisions with an activation barrier.¹⁰ The activation energy is assumed to be equal to the energy required to excite one Fe atom to its first excited state. The rate coefficient is obtained from the expression¹⁰

$$k(T) = \pi d^2 \sqrt{\frac{8kT}{\pi m_1}} \exp\left(-\frac{E_a}{kT}\right) \quad (2)$$

where πd^2 is the cross section of Fe atoms (determined from bulk average diameter), m_1 is the mass of Fe atoms, and E_a is the threshold energy for the reaction, assumed to be about 7000 1/cm. ($\sim 10,000$ K). Should it be necessary to excite both atoms, the activation energy would be double the one considered here and the nucleation rate would be virtually zero. The temperature dependence of these various nucleation rates is shown in Figure 2.

2.3.4. Cluster Growth and Evaporation. Most of the Fe cluster growth and evaporation reaction rates were obtained from cluster theory. In the Ames preliminary model the rates are assumed to be constant after a given size cluster. In the Girshick-based model, the rates were determined from collision frequencies estimated from the cluster size, assuming spherical symmetry. The expressions for growth β_{ij} and evaporation E_j , respectively, are

$$\beta_{ij} = \left(\frac{3\nu_1}{4\pi}\right)^{1/6} \sqrt{\frac{6kT}{\rho_p} \left(\frac{1}{i} + \frac{1}{j}\right)} (i^{1/3} + j^{1/3})^2 \quad (3)$$

$$E_j = \beta_{1,j-1} n_s \exp(\Theta [j^{2/3} - (j-1)^{2/3}]) \quad (4)$$

where $\Theta = \sigma s_1/kT$ is the dimensionless surface energy, ν_1 is the hard-sphere collision frequency of monomers, ρ_p is the density of bulk iron, i and j are the number of atoms in the colliding clusters, σ is the surface tension of Fe, s_1 is the surface area of the monomer (iron atom), k is the Boltzmann constant, and T is the temperature. The saturation number density, n_s , is a function of temperature given by a Clausius-Claperon type relation.

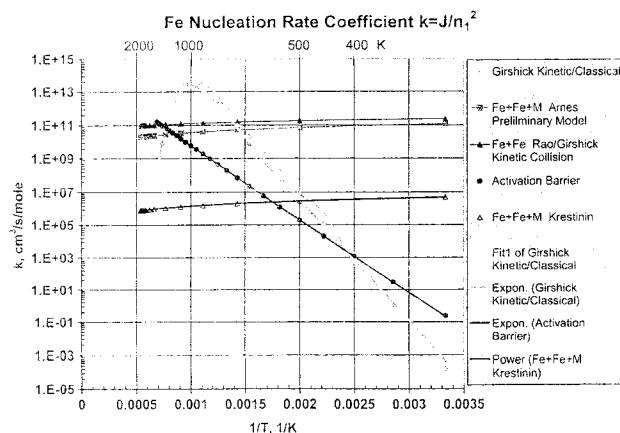
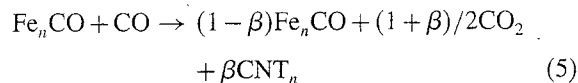


Fig. 2. Comparison of various Fe nucleation rate coefficients versus temperature.

2.3.5. Formation/Growth of Carbon Nanotubes. Carbon nanotubes form from the reaction of CO with Fe_nCO clusters. These Boudouard reactions are expressed in stoichiometrically balanced form as



where $\beta = 1/(2N_c - 1)$ and N_c = number of carbon atoms in the SWNT.

The reaction for growing SWNTs (CNT_n) in the Ames preliminary model assumed that an average-sized SWNT is 3000 carbon atoms long, but in the present calculations, only 999 are assumed. The number of atoms in any given species is limited to 999 by the input format of three digits for number of atoms per element limits. These calculations do not consider growth of nanotubes by sequential addition of carbon, such as $\text{Fe}_n\text{C}_{872} + \text{CO} \Rightarrow \text{Fe}_n\text{C}_{873} + \frac{1}{2}\text{CO}_2$. The growth is assumed to occur by the fraction β carbon nanotubes per $\text{Fe}_n\text{CO} + \text{CO}$ reaction. The format of the CHEMKIN code used for the description of species allows up to four elements (NASA table thermodynamic property format).¹¹ In the case where 2048 Fe atoms is assumed, it is required that Fe be listed three times in the description of the molecule. For example, Fe_{2048} could be represented as $\text{Fe}_{999}\text{Fe}_{999}\text{Fe}_{50}$. The reaction rate coefficient for CNT_n formation was estimated from literature values for Fe and similar catalysts.^{12,13}

3. RESULTS AND DISCUSSION

The chemical rate equations are solved for two situations. The first application simulates the mixing and evolution of $\text{Fe}(\text{CO})_5$ with hot CO in the shower head and flow reactor (but without a change in the total iron concentration due to dilution by CO). The second set simulates conditions in which iron pentacarbonyl is assumed to be dissociated before injection into the hot reactor, say by a laser. Dilution of $\text{Fe}(\text{CO})_5$ in N_2 and CO is considered. Again, the change in fraction of total iron due to mixing is not considered because of limitations in the SENKIN code.

3.1. Full Flow Simulations Along Streamlines

The simulations of the production of SWNTs in the HiPco apparatus use the temperatures determined from the FLUENT flow field solutions. Injection of cold catalyst and CO into the shower head and mixing with hot CO results in highly recirculating, three-dimensional turbulent flow. An example of several trajectories is given in Figure 3. As can be seen, some of the flow lines recirculate before leaving the mixing zone, whereas others (the ones near the centerline) exit without circulation. The chemical rate equations, as modeled in Table I and its variations, are solved. In the present paper, kinetics calculations are

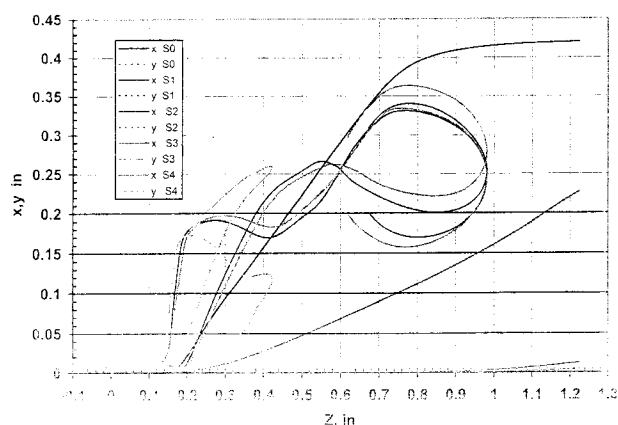


Fig. 3. x and y coordinates along four typical streamlines versus the axial coordinate z , in mixing zone of HiPco reactor, calculated by the FLUENT code.

shown for a case near the centerline. This streamline was arbitrarily chosen from another flow field solution to demonstrate the method. Its temperature history is given in Figure 4. Since only the first few centimeters of the flow reactor are simulated in the FLUENT solutions, the flow in the rest of the flow tube is assumed to remain at a constant temperature and pressure until its end (about 20 cm). The temperature then ramps down to ambient and then remains constant until the end of the calculation, arbitrarily taken as 1 s. It turned out that most of the significant chemistry occurs within the first 500 μ s, or a distance of about 1.5 cm for the streamline considered. In the trajectory considered here the temperature remains about 1150 K until 80 ms, at which time the temperature ramps down to ambient. At 80 ms the number and distribution of SWNTs have reached steady values, as seen in Figure 5, which shows the time evolution of selected-size SWNT clusters with various assumptions of the nucleation rate. These cases are for the $n_{\max} = 40$ cluster model (Table Ib). For all assumed nucleation rates, the total nanotube population has reached a steady value by 10 ms. We see that SWNTs start growing as soon as the temperature has reached about 1100 K. Figure 5 also shows a faster rise in SWNT population with fast

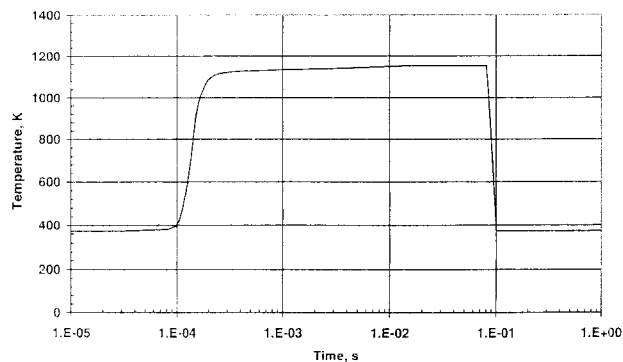


Fig. 4. Temperature history along trajectory inj0 streamline.

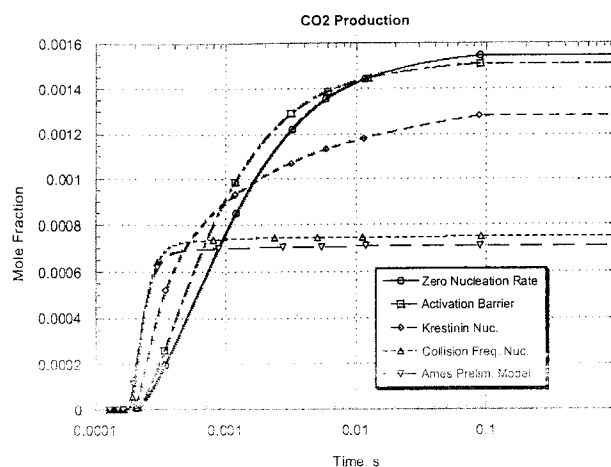


Fig. 5. Calculated evolution of total SWNT (also equals CO_2) mole fraction for trajectory inj0 with 40-Fe-atom cluster model and various nucleation models.

nucleation of Fe atoms. However, the ultimate production of SWNTs does not seem to depend much on the nucleation rate. The origin of clusters on which CO reacts to form SWNTs is somewhat obscure. Direct dimer formation from Fe atoms may be a slow reaction; and there is the possibility that the reaction to form Fe_2 from two FeCO molecules may be significant. These possibilities will be discussed in a later section.

3.2. Cluster and Nucleation Model Comparison

The three models given in Table I were used to compute the evolution of the species in the reactor. Solutions obtained assuming these models exhibit quite different behavior.

3.2.1. Ames Preliminary 200-Atom Cluster Model.

At the end of the reactor the population of cluster sizes in the 971-species Ames model with clusters up to $n = 200$ decreases with cluster size. There are very few large clusters. This results from cluster growth from the addition of only small Fe clusters (Fe , Fe_2 , Fe_3 , and Fe_4). Indeed, calculations show that with a model truncated to, say, $n_{\max} = 50$, the distribution is only slightly affected. The cluster size distributions for the Ames 200-atom-cluster model (Table Ia) is shown in Figure 6 for times of 80 ms and 1 s. We can see that there are almost no appreciable clusters greater than $n = 25$. In addition, no dead nanotubes (DCNT_n) are seen in the results because the assumed reaction rate coefficients needed to convert Fe_nCNTs to DCNT_n s are very small, $k = 1 \text{ cm}^3/\text{s/mol}$. This model, therefore, has limits, since we know from transmission electron micrographs² (TEMs) that iron clusters of up to several thousand atoms exist in the product. We can also see that by 80 ms the distribution no longer changes, even as late as 1 s, after the flow has exited the reactor. The

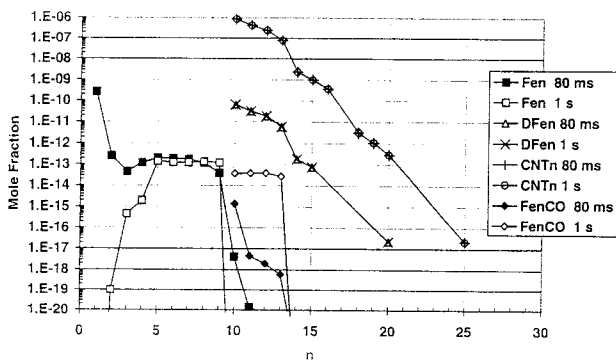
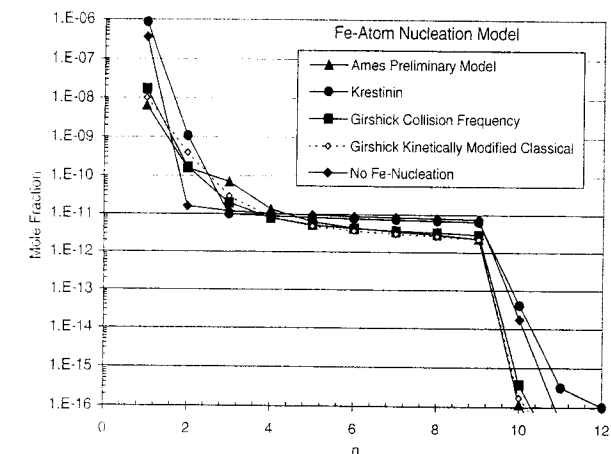


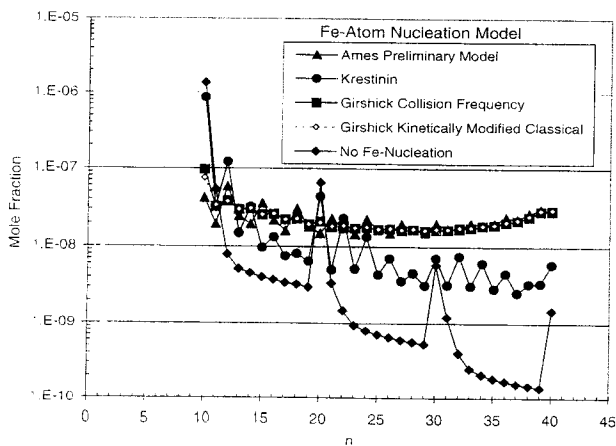
Fig. 6. Cluster size distribution for the Ames preliminary 200-atom cluster model at 80 ms and 1 s in trajectory inj0.

main change is that small Fe molecules are converted to Fe_nCO .

3.2.2. 40-Atom Cluster Model. The population of SWNTs and other clusters at 80 ms for the 40-atom cluster model is shown in Figure 7. Coagulation of larger clusters has a significant effect on the cluster size distribution.



(a)



(b)

Fig. 7. Cluster size distribution for the 40-atom cluster model at 80 ms in trajectory inj0. (a) Iron clusters, Fe_n . (b) SWNTs, CNT_n .

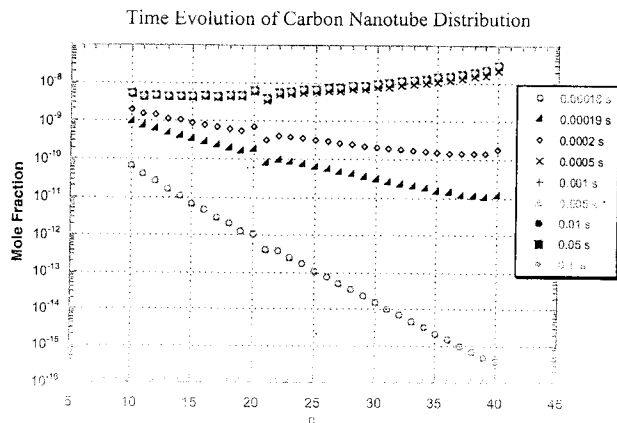


Fig. 8. Evolution of SWNT distribution for the 40-atom cluster model in trajectory inj0.

The population of SWNTs is fairly flat and tends to increase to the maximum at $n = 40$. Had a larger maximum size cluster been chosen, we would probably see the distribution reach a maximum and then fall off for the largest clusters. The particular nucleation model chosen affects some of the species significantly, particularly the distribution of SWNTs, but not the total number. The evolution of the distribution of SWNTs and Fe_nCO clusters does not change much after 500 μs , as can be seen in Figures 8 and 9, respectively. If the nucleation rate is very slow or zero, then the formation of larger SWNTs is reduced significantly, provided there is no other means of forming Fe_2 . However, there is a pathway of forming Fe_2 other than from Fe atom recombination. Upon decomposition of $Fe(CO)_5$, we obtain $FeCO$ molecules, which may collide with Fe to form Fe_2 and CO molecules. If this reaction is eliminated from the reaction set, we obtain very little production of SWNTs and CO_2 . Table II compares the production of CO_2 and the percentage of iron at the exit of the reactor. We see that unless one of these two reactions is included, CO_2 production is low and the

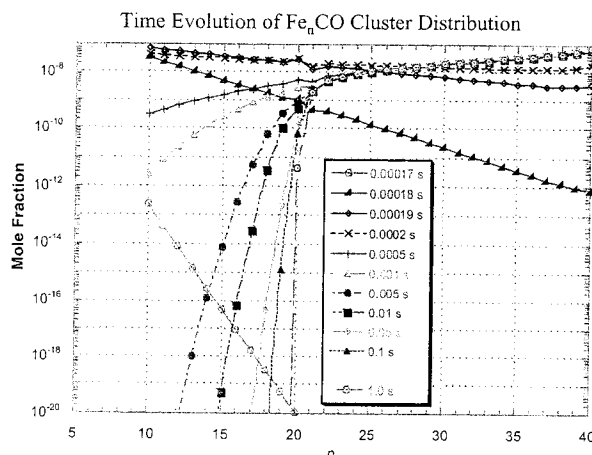


Fig. 9. Evolution of Fe_nCO distribution for the 40-atom cluster model in trajectory inj0.

Table II. Effect of Fe Nucleation on Efficiency, as Evaluated from Production of CO₂ and Percentage of Iron at 1 s in Trajectory (inj0) for the 40-Atom Cluster Model with Girshick Cluster Rates.

Nucleation model	Included $\text{Fe} + \text{FeCO} \rightarrow \text{Fe}_2 + \text{CO}$	wt% Fe	CO ₂ mole fraction
Zero nucleation	Yes	4.88	1.54×10^{-3}
Zero nucleation	No	93.66	5.36×10^{-6}
Nucleation at collision frequency	Yes	9.58	7.48×10^{-4}
Nucleation at collision frequency	No	9.54	7.52×10^{-4}
Krestinin rate	Yes	5.50	1.36×10^{-3}
Hard sphere with activation barrier	Yes	4.99	1.51×10^{-3}
Girshick kinetic model of classical theory	Yes	9.74	7.34×10^{-4}
Ames prelim. model nucleation	Yes	10.08	7.07×10^{-4}

percentage of iron is large. It is interesting to note that at zero nucleation (no $\text{Fe} + \text{Fe} \rightarrow \text{Fe}_2$) there is a greater production of carbon and a lower percentage of iron in the product. This may be due to the effect that delayed Fe cluster formation delays the formation of SWNTs until the temperature is higher and the rate coefficient for their formation is higher. The 40-atom cluster model does not admit clusters as large as seen in the product. Therefore, the following model is considered.

3.2.3. 2048-Atom Grouped Cluster Model. Because the 40-atom model is arbitrarily truncated to a size much smaller than that of the clusters observed in the HiPco reactor after production, it is desirable to account for larger clusters in the model. However, the time required to compute the chemical rate equations increases with the number of species squared; a very large model of thousands of species would be virtually prohibitive in terms of computer time and possibly accuracy. In an attempt to reduce the size of the model, yet allow for large clusters, a reduced or grouped model was developed. The rates in this model are based on Girshick's cluster growth, Eq. (3). However, since we do not include species of every size, reaction rates for lumped species are multiplied by the number of species they represent. This factor is applied to both formation and evaporation rate coefficients for iron clusters.

The results of the solution of the rate equations along the streamline (denoted inj0) at 1 s are given in Figure 10, where we show the effect of the different nucleation models. Slow nucleation of Fe tends to delay the formation of larger clusters, but the total number of clusters is not reduced significantly. With slow nucleation, more of the Fe_nCO clusters and CNT_n is in the low n range. Since experimentally we see larger clusters (perhaps because they are more visible in TEM) it appears that the nucleation rate must be rather fast and that agglomeration is important. Figure 11 shows the evolution of the cluster distribution for the 2048-atom grouped model with Krestinin nucleation rates. As in the 40-atom model, the production of large clusters evolves very quickly and levels off at a time between 220 and 300 μs . The largest SWNT cluster, CNT_{2048} , is more highly populated than the next smaller one, indicating that even $n = 2048$ is probably too small.

3.3. Production of CO₂ and Carbon: Comparison with Experiment

To assess how well the models predict experimental results, a comparison was made of the amount of CO₂ produced and the amounts of iron relative to carbon at the exit of the reactor. The concentration of CO₂ in the exhaust from the reactor was measured by gas chromatography and mass spectrometry. The amount of iron in the final product was measured by thermogravimetric analysis (TGA) by heating a sample in air to burn away the carbon and measuring its weight loss. The remaining material is assumed to be iron oxide. The rate of carbon production can be determined from the CO₂ measurements; and from the flow rate of CO and $\text{Fe}(\text{CO})_5$, one can determine the amount of carbon produced and iron consumed. To determine how much iron is predicted by the simulations we computed the total mass fraction of Fe based on the mole fractions of all species at the end of the calculation. The amount of CO₂ concentration is given in Figure 12, and the fraction of Fe in the product is given in Figure 13. We see from these figures that the computations yield higher efficiency than reality. We must provide the caveat that the production is based on a single representative streamline. Production of CO₂ may be different along different streamlines. Therefore, these calculations should only be

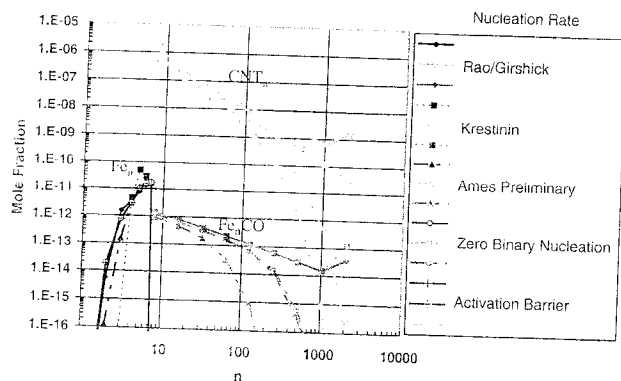


Fig. 10. Cluster size distribution for the 2048-atom grouped cluster model at 1 s in trajectory inj0. Various nucleation models are compared, including no direct Fe nucleation.

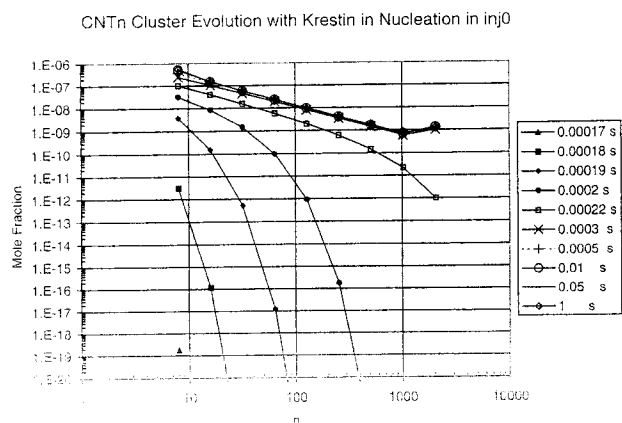


Fig. 11. Evolution of SWNT distribution for the 2048-atom cluster model with Krestinin Fe nucleation rate in trajectory inj0.

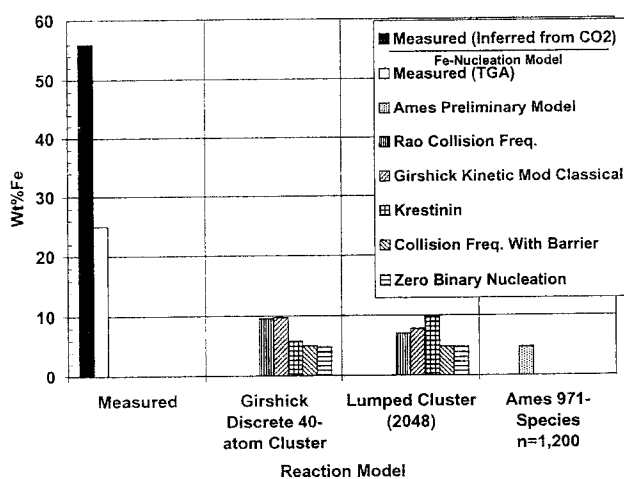


Fig. 12. Histogram of amount of carbon produced by the Boudouard reaction in a HiPco reactor for various models and assumptions about iron nucleation rates. The amount of carbon is based on the mole fraction of CO₂ at the end of the process.

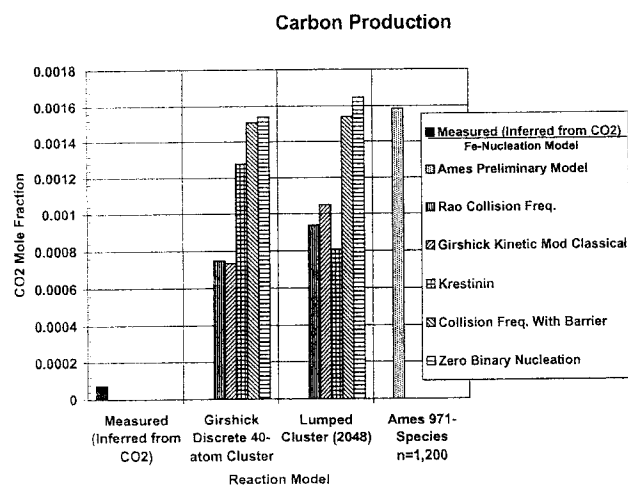


Fig. 13. Histogram of iron content at the end of the process in the HiPco reactor for various models and assumptions about iron nucleation rates.

used for relative comparisons. The measured amount of carbon produced is over an order of magnitude lower than calculated. The measured iron content is 5 to 10 times that calculated, depending on the particular model. This may be due to the rate coefficients chosen for the Boudouard disproportionation reaction being higher than reality. The average number of carbon atoms assumed to be in a CNT affects the rate of production of CNTs. Because of the nature of the CHEMKIN code, it is difficult to calculate the growth of chain molecules such as SWNTs or polymers without defining a separate species for each length of chain. Models are restricted to reactions that balance stoichiometrically. (It may be possible to determine growth rates, however.) There is not much difference in the different cases except for one: the 40-atom cluster model with Girshick kinetically modified classical nucleation. The nucleation rate does not significantly affect the results because $Fe + FeCO \Rightarrow Fe_2 + CO$ is a pathway to forming Fe₂. Fe₂ then can react with Fe and other species to grow larger Fe clusters.

3.4. Evolution of Iron Vapor in the Incubation Region before Injection into the Reactor

A modification of the apparatus has been proposed in which iron clusters are formed before injection into the shower head. A laser of 514-nm wavelength can photodissociate Fe(CO)₅ and subsequent carbonyls into Fe and CO. The Fe atoms, diluted in an inert gas such as nitrogen, may then form iron clusters at low temperature. To assess this possibility several solutions of the chemical rate equations were obtained with various assumptions about the rate of nucleation as well as assumptions about the concentration of CO, N₂, and Fe(CO)₅. It was found that relaxation of Fe in pure CO results in mostly Fe(CO)₅ and very few iron clusters, but if nitrogen is used, the number of iron clusters is much greater. The effect of nucleation rate is shown in Figure 14. We see that for very low nucleation rates (zero and the threshold model rates) there are a large number of Fe atoms, but not many pure Fe clusters. Clusters as large as Fe₈CO are relatively larger than for higher nucleation rates, but the largest cluster, Fe₂₀₄₈, is larger, but not as large as when the nucleation rate is high (Krestinin, Ames Preliminary, and Rao/Girshick rates, respectively) as seen in Figure 14. Apparently, when the nucleation rate is low the only mechanism for forming clusters is the reaction $Fe + FeCO \Rightarrow Fe_2 + CO$. This slows the evolution of larger clusters.

As for the effect of CO concentration in N₂, the calculations show that for CO concentrations up to about 10% the distribution of Fe_nCO clusters is about the same. Figure 15 shows that their number and distribution do not depend significantly on the concentration of CO at low concentrations. Numerically, even the distribution of Fe

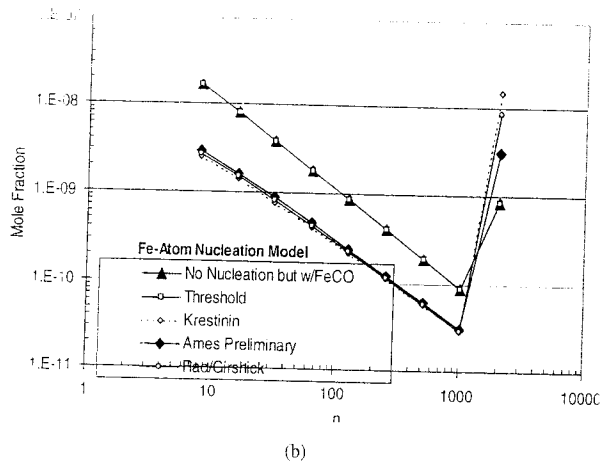
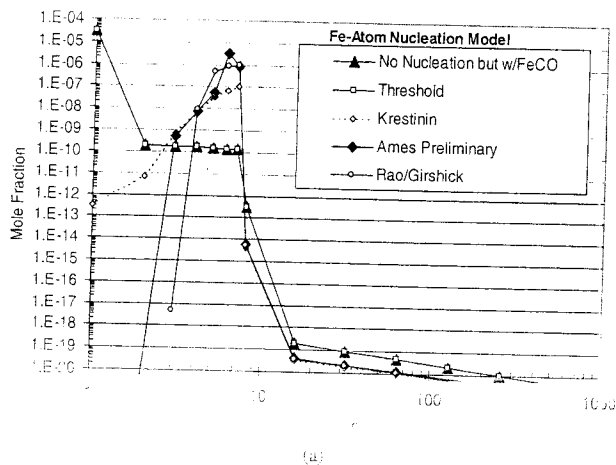


Fig. 14. Effect of nucleation assumption on cluster distribution in incubation region at 0.5 ms and 400 K and 35 atmospheres. Also shown are comparisons of solutions with zero Fe-nucleation and without the $Fe + FeCO \Rightarrow Fe_2 + CO$ exchange reaction. (A) Iron clusters, Fe_n . (B) SWNTs, CNT_n .

clusters is about the same if there were no CO in the mixture, that is, the initial mixture consists of Fe and N_2 only (no CO and no iron pentacarbonyl). It is also seen that if pure Fe is diluted, at the end of a relaxation time of

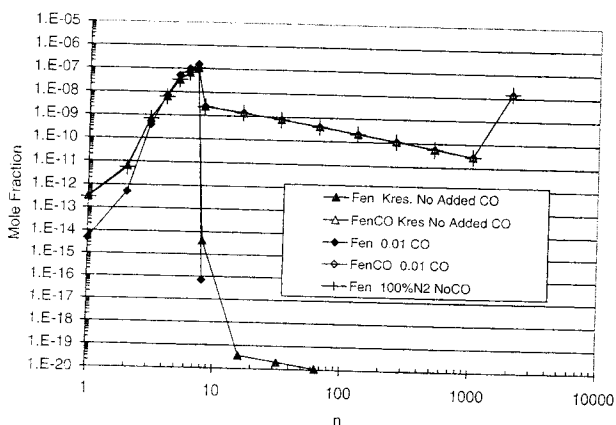


Fig. 15. Effect of the nucleation model on the distribution of lumped clusters in 400 K and 35 atm incubation section at 0.5 ms with 32 ppm Fe and 32 ppm CO, except where noted: 2048-atom cluster model.

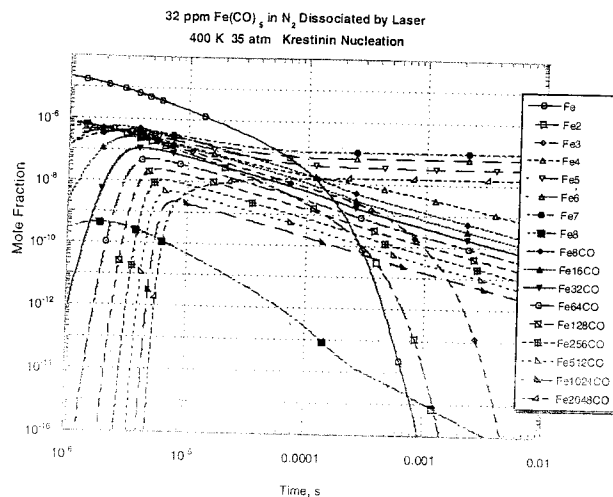


Fig. 16. Time history of clusters in the incubation region at 400 K and 35 atmospheres with 32 ppm Fe in N_2 . Krestinin nucleation rates assumed: 2048-atom cluster model.

0.5 ms the Fe_n distribution is nearly the same as the one where the CO concentration is low, except that the Fe_n clusters have no CO attached.

The time evolution of iron and Fe_nCO clusters in the incubator is shown in Figure 16, where Krestinin's nucleation rate is assumed. It turns out that at 400 K and 35 atm, with not too great an amount of CO, nucleation does not affect the results very much. However, to allow for sufficient growth, but not too much agglomeration, one needs to determine the length of the incubator, based on velocity and time desired. This relation is given in Figure 17. For the experimental condition in which 42 slm is injected into the reactor through a 1-mm-radius tube, the velocity is about 38 m/s. For this condition, it takes 0.5 ms for the flow to go 2 cm, as seen in Figure 16. Two centimeters is a nominal distance through which one might want to fire a laser to dissociate iron pentacarbonyl. A 20-Hz laser would illuminate a 2-cm-long volume of gas with each firing, after which the gas would enter the reactor before the next laser pulse.

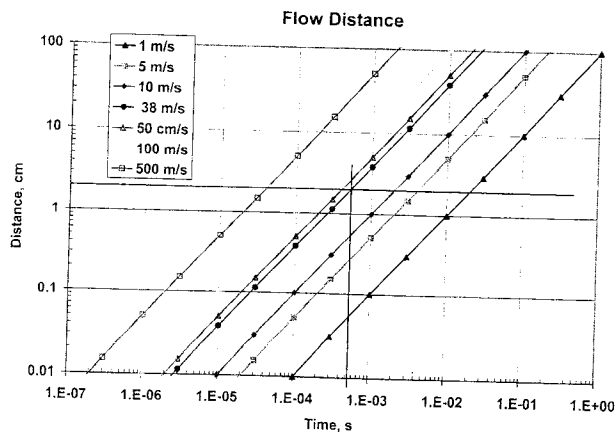


Fig. 17. Distance vs. time relation for various velocities in an incubation tube.

4. CONCLUSIONS

Solutions to the chemical rate equations were obtained with the SENKIN code of the CHEMKIN package to find the production of single-wall carbon nanotubes and precursor iron clusters. Various assumptions of nucleation rates and cluster models were studied. It was found that the nucleation rate did not affect the production of CNTs very much, since Fe dimers are also formed by the exchange of Fe for CO from FeCO. Three cluster models were investigated; one allowed clusters up to $n = 200$ but only allowed growth by accretion of Fe to Fe_n to the clusters. Two other models were considered in which larger clusters could merge or form clusters. The first considered all sizes up to Fe₄₀ and Fe₄₀CO. The second lumped clusters into discrete groups of $n = 2^x$, where $x = 3, 11$ ($n_{\text{max}} = 2048$). The reaction rate coefficients were adjusted to account for missing clusters. This model allowed for much larger clusters, as seen in the measurements.

For all models studied the simulations of the reactor overpredicted the amount of SWNT and CO₂ produced. This may be related to the assumed rate coefficients for the formation of SWNTs, which were the same in all of the models.

A proposed formation of iron clusters before injection into the heated reactor was investigated to determine the cluster size distribution and evolution if the initial Fe is produced instantaneously by a laser dissociation of iron pentacarbonyl. The results were useful in assessing the mechanism for the nucleation of iron. It was found that the nucleation rate did not affect the cluster formation

since exchange of Fe with CO when colliding with FeCO would produce sufficient Fe₂ to initiate cluster formation at low temperatures and presumably at high temperatures as well. The distribution of clusters was also insensitive to the mixture dilution up to 10% CO in N₂.

Acknowledgments: The authors thank Drs. Michael Bronikowski and Pavel Nikolaev for helpful discussions about the operating conditions of the HiPco apparatus.

References and Notes

1. P. Nikolaev, M. J. Bronikowski, R. K. Bradley, F. Rohmund, D. T. Colbert, K. A. Smith, and R. E. Smalley, *Chem. Phys. Lett.* 313, 91 (1999).
2. M. J. Bronikowski, P. A. Willis, D. T. Colbert, K. A. Smith, and R. E. Smalley, *J. Vac. Sci. Technol.* 19, 1800 (2001).
3. A. Povitsky, *Comput. Fluids* 31, 954 (2002).
4. A. Povitsky and M. Salas, ICASE Report 2001-04, NASA CR 2001-210662 (February 2001).
5. A. E. Lutz, R. J. Kee, and J. A. Miller, Sandia National Laboratories Report 97-8248 (1988).
6. C. E. Dateo, T. Gökçen, and M. Meyyappan, *J. Nanosci. Nanotechnol.* 2, 523 (2002).
7. N. Rao, S. Girshick, J. Heberlein, P. McMurry, S. Jones, D. Hansen, and B. Micheel, *Plasma Chem. Plasma Process.* 15, 581 (1995).
8. D. M. Cox, K. C. Reichmann, D. J. Trevor, and A. Kaldor, *J. Chem. Phys.* 88, 111 (1988).
9. A. V. Krestinin, V. N. Smirnov, and I. S. Zaslono, *Sov. J. Chem. Phys.* 8, 689 (1991).
10. R. D. Levine and R. B. Bernstein, *Molecular Reaction Dynamics*, Oxford University Press, New York (1974).
11. S. Gordon and B. J. McBride, NASA Report SP-273 (1971).
12. L. J. Whitman, L. J. Richter, Bruce A. Gurney, J. S. Villarrubia, and W. Ho, *J. Chem. Phys.* 90, 2050 (1989).
13. B. P. Jalan and R. K. Rao, *Carbon* 16, 175 (1978).

Received: 6 July 2002. Revised/Accepted: 21 November 2002.